Heat transport in a non-homothermal turbulent particle-laden flow in the collisional regime

Heat transport in a non-homothermal turbulent particle-laden flow in the collisional regime

Journal of Physics: Conference Series **2685** (2024) 012002 doi:10.1088/1742-6596/2685/1/012002

Heat transport in a non-homothermal turbulent particle-laden flow in the collisional regime

Hamid Reza Zandi Pour* **and Michele Iovieno**

Dipartimento di Ingegneria Meccanica e Aerospaziale, Politecnico di Torino,
Corso Duca degli Abruzzi 24, 10129 Torino, Italy

* Corresponding author: hamid.zandipour@polito.it

Abstract. In this investigation, we explore the impact of particle collisions on turbulent heat flux within a temporally developing thermal mixing layer arising from the interaction of two homothermal regions driven by a statistically homogeneous and isotropic velocity field. Employing two-way thermally coupled Eulerian-Lagrangian Direct Numerical Simulations (DNSs) at a Taylor microscale Reynolds number up to 124, we examine the influence of particle collisions for a Stokes number from 0.2 to 3, maintaining a fixed thermal to kinetic relaxation times ratio of 4.43. Our study quantifies the reduction in average heat transport induced by particle-to-particle collisions, which disrupt the temperature-velocity correlation created by the initial temperature difference. Notably, while collisions diminish this correlation, our analysis reveals their overall impact remains minor, even at the highest simulated Stokes number. Additionally, we present statistics of the temperature difference among colliding particles across various flow conditions.

1. Introduction

The ubiquity of particle-laden flows in almost every application makes them a still very active field of research for many disciplines. Furthermore, the mechanical and thermal impacts of inter-particle collisions in several industrial and natural turbulent flows carrying inertial heavy particles play a significant role even in dilute regimes. For instance, understanding the droplet collisions in clouds and particle-particle collisions in sandstorms are essential in order to study these multi-physics phenomena [1]. Given the difficulties of Lagrangian measurements, in particular when the thermal interplay between the two phases is considered, a lot of insight has been obtained through numerical simulations. Fluid-particle thermal interplay has been studied mostly under the point particle assumption, which is valid for particles much smaller than Kolmogorov size, both in wall-bounded turbulent flows [2, 3, 4] and in homogeneous turbulent regimes [5, 6, 7].

Saffman and Turner [8] developed the theory for small droplet collision in clouds. They found that collision rate of identical sub-Kolmogorov droplets depends only on the turbulent dissipation rate, fluid viscosity and droplet radius, and they also showed that the collision frequency is independent of droplet thermophysical properties. The effect of particle parameters such as particle response time, number density and size on collision rate was investigated by Sundaram and Collins. They found that collision rate depends highly on Stokes number [9]. Moreover, some other works have studied the inter-particle collision effect in particulate turbulent flow by developing kinetic-based methods [10, 11, 12, 13]. In the last decade some works have extensively studied the impact of particle-particle collision along with particle-wall collision in the wall-bounded flows [14, 15].

Collisions between particles influence drastically the transport of heat in solid-fuel combustors, because particles much denser than the fluid can escape the near-wall zone, thus transferring heat

between the boundaries and zones away from the wall. Even if the volume fraction of these applications usually is far above the validity range of the two-way coupling regime, and often beyond the validity of point-particles approach, [16], they suggest that fluid-particle thermal interactions can lead to a significant modification of the ability of a flow to transport heat also in dilute suspensions. The impact of collisions is normally not considered, when heat transfer is under investigation, even if it is evident that at such high volume fractions the collisions likelihood increases leading to collision-induced heat transfer modifications. There exist only a small number of theoretical studies involving collisions, like the work of [17] who assesses in an analytical way the heat transfer during a non-instantaneous elastic collision event with a solid wall. Carbone et al. [6] have assessed the effect of inter-particle collisions on the fluid temperature structure functions in isotropic turbulence when particles are one-way thermally coupled, showing that temperature statistics at small-scale barely are influenced by collisions. However, collisions reduce the acceleration of small particles while large particles are accelerated more, resulting in intensified velocity scattering. When a high fluid temperature gradient exists, such scattering may enable them not only to transfer heat near their position, but also to transfer heat to regions quite distant from their neighbourhood. This mechanism is responsible for a heat transfer enhancement in two-phase particulate flow by amplifying the interphase exchange of heat between two phases along particle Lagrangian trajectories [18], even in presence of an isotropic velocity field. Recently we have studied the thermal interplay of fluid and particle in a non-isothermal flow. This basic configuration is also suitable to be employed to improve the existing turbulence models of two-phase flows. One- and two-way thermally coupled particle-laden flows have been numerically investigated [18] in a dilute particulate flow without considering inter-particle interaction.

To explore the contribution to the heat transport of colliding particles in dilute suspension, we carry out Eulerian-Lagrangian DNSs to analyze the effect in the heat transport of non-cohesive collisions between particles in the two-way thermally coupled regime in the simplest inhomogeneous flow configuration, the time-evolving mixing layer between two regions at a different temperature subject to a homogeneous and isotropic turbulent velocity field. We complement our previous work [18] by examining the role of collisions for Stokes numbers from 0.2 to 3, for particles with a ratio between momentum and thermal relaxation times is fixed as 4.43, in a flow with a Reynolds number based on Taylor microscale up to 124. We quantify the extent to which particle collisions attenuate the average heat transfer relative to the flow regime with non-colliding particles and demonstrate that the overall impact is insubstantial even for large inertial particles. We compare our findings with the same flow configuration in absence of collisions, so that the statistics presented in [18] are used a baseline, providing valuable insights into the effects of the collisions among particles. We show that collisions bring a reduction of particle temperature variance with respect to fluid temperature variance, while fluid-to-fluid and particle-to-particle variance ratios slightly increase by collisions especially when particle inertia increases. Due to particle thermal back reaction, collisions increase the variance of the temperature of the carrier flow higher than the one of the particles, especially at the highest simulated Stokes numbers, even if the difference is small and it could become considerable only at a much higher volume fractions [19]. The ability of inertial particles to carry heat to zones distant from their position is indicated also by the mean temperature difference between colliding particles conditioned over the normalized position across the mixing layer.

2. Physical model

2.1. Governing equations

Within the Eulerian-Lagrngian method, the motion of a non-homothermal divergence-free flow seeded by small heavy inertial particles is governed by the Navier-Stokes equations coupled with the Lagrangian equations for the dynamics of discrete particles. Temperature variations are assumed small enough not to be producing relevant density changes, so that temperature behaves as an advected passive scalar. Hence,

the continuous fluid phase field equations are

$$\partial_i u_i = 0 \tag{1}$$

$$\partial_t u_i + u_j \partial_j u_i = -(1/\rho_0)\partial_i p + \nu \partial_j \partial_j u_i + f_{u,i}, \tag{2}$$

$$\partial_t T + u_j \partial_j T = \kappa \partial_j \partial_j T + (1/\rho_0 c_{p0}) C_T. \tag{3}$$

Here $\boldsymbol{u}(t,\boldsymbol{x})$, $p(t,\boldsymbol{x})$, and $T(t,\boldsymbol{x})$ are fluid velocity, pressure, and temperature, while the (constant) fluid density, kinematic viscosity, thermal diffusivity and isobaric specific heat capacity are denoted by ρ_0, ν, κ, and c_{p0}. Additionally, $\boldsymbol{f}_u(t,\boldsymbol{x})$ is an external force on the fluid imposed to keep the velocity of the carrier fluid in a statistically steady state, while C_T is the fluid-particle interphase heat transfer per unit mass per unit time. No particle momentum feedback has been taken into account, as in [18, 19, 20], because, as shown in [6], in a dilute suspension it has a insignificant impact on temperature statistics. Particles are modelled as non-deformable spheres whose radius R is much smaller than the turbulence dissipation lengthscale η (i.e. Kolmogorov microscale), so that it's possible to consider them as material points. When their density is much higher than the fluid density, their motion is dominated by the Stokes drag, allowing to neglect all other forces in the Maxey-Riley equation [21]. By using analogous arguments, an equation for the evolution of the temperature of small particles, with a Biot number much smaller than unity, can be derived, thus leading to the following system of equations,

$$\frac{\mathrm{d}^2 \boldsymbol{x}_p}{\mathrm{d}\,t^2} = \frac{\mathrm{d}\boldsymbol{v}_p}{\mathrm{d}\,t} = \frac{\boldsymbol{u}(t,\boldsymbol{x}_p) - \boldsymbol{v}_p}{\tau_v}, \qquad \frac{\mathrm{d}\vartheta_p}{\mathrm{d}\,t} = \frac{T(\boldsymbol{x}_p,t) - \vartheta_p}{\tau_\vartheta}, \tag{4}$$

where $\boldsymbol{x}_p(t)$, $\boldsymbol{v}_p(t)$ and $\vartheta_p(t)$ are the the position, velocity and temperature of the p-th particle. Coefficients τ_v and τ_ϑ in equation (4) are the momentum and temperature relaxation times of particles, defined by

$$\tau_v = \frac{2}{9}\frac{\rho_p}{\rho_0}\frac{R^2}{\nu}, \qquad \tau_\vartheta = \frac{1}{3}\frac{\rho_p c_{pp}}{\rho_0 c_{p0}}\frac{R^2}{\kappa}, \tag{5}$$

where the density of a single particle is ρ_p and c_{pp} denotes its specific heat at constant pressure. Collisions are the only direct particle-particle interaction that is included in this study. Thus, the particle back reaction per unit volume per unit time on the fluid temperature field reads

$$C_T(t,\boldsymbol{x}) = \frac{4}{3}\pi R^3 \rho_p c_{pp} \sum_{p=1}^{N_p} \frac{\mathrm{d}\vartheta_p(t)}{\mathrm{d}t}\delta(\boldsymbol{x} - \boldsymbol{x}_p). \tag{6}$$

2.2. Numerical method and setup

The main objective of this work is the turbulent transport of heat occurring at the interface between two flow regions which are subject to homogeneous and isotropic turbulence with uniform temperatures, viz. T_1 and $T_2 < T_1$. To simulate it, the governing equations presented in Section 2.1 are numerically solved within a parallelepiped domain with dimensions $L_1 = L_2$ and $L_3 = 2L_1$ along the x_1, x_2, and x_3 directions. We set the initial temperature be be equal to T_1 in the $x_3 < L_3/2$ half-domain and equal to T_2 in the other half domain, $x_3 > L_3/2$. Temperature of both fluid and particles is decomposed into the sum of a linear part $T_1 + (T_2 - T_1)(x_3/L_3)$ and a residual part, following [18], so that periodicity can be imposed on the residual part, while particles which exit the domain reenter on the opposite side with the same residual temperature.

Equations (1-6) are rendered non-dimensional by using as reference the length $L_1/(2\pi)$, a velocity scale derived from ε, the kinetic energy dissipation rate imposed by the forcing, and the temperature difference $T_1 - T_2$ between the two zones, as described in detail in [18]. To make results more physically insightful,

the Taylor microscale λ is used as reference length in the definition of dimensionless parameters, so that, in the adimensional form, the flow is governed by the Reynolds number $\mathrm{Re} = u'\lambda/\nu$, the Prandtl number $\mathrm{Pr} = \nu/\kappa$, and the thermal mass fraction $\varphi_\vartheta = \varphi(\rho_p c_{pp})/(\rho_0 c_{p0})$, where φ denotes the volume fraction of particles. Analogously, it is more insightful to relate the particle relaxation times, the only dimensional parameters in particle equations, to the timescale of small-scale fluid fluctuations, the Kolmogorov timescale $\tau_\eta = (\nu/\varepsilon)^{1/2}$, more than to the adimensionalization timescale, so that their dynamics is governed by the small scale Stokes number $\mathrm{St} = \tau_v/\tau_\eta$ and thermal stokes number $\mathrm{St}_\vartheta = \tau_\vartheta/\tau_\eta$. All simulations have been performed at the same volume fraction $\varphi = 4 \times 10^{-4}$, with $\rho_p/\rho_0 = 1000$, $c_{pp}/c_{p0} = 4.16$, $\mathrm{Pr} = 0.71$, so that $\mathrm{St}_\vartheta/\mathrm{St} = 4.43$, and, in dimensionless form, $\tau_\eta = 0.098$, $\eta = 0.0153$, $\varepsilon = 0.25$. We carried out three different sets of simulations with Taylor Reynolds number $\mathrm{Re}_\lambda = 56$, 86, 124 by forcing wavenumber $\kappa_f = 5, \sqrt{6}, \sqrt{3}$ respectively. Their corresponding dimensionless integral lengthscale, Taylor lengthscale and velocity fluctuation root mean square are respectively $\ell = 0.4$, 0.74, 0.94, $\lambda = 0.226$, 0.290, 0.350, and $u' = 0.59$, 0.71, 0.85. In addition, we have carried out simulations over a large range of Stokes numbers, from 0.2 to 3. A pseudospectral method, fully dealiased with the 3/2 rule, has been used to discretize the carrier flow equations (1–3). A linear deterministic forcing $\boldsymbol{f}_u$, given in the Fourier space by

$$\hat{f}_{u,i}(t,\boldsymbol{\kappa}) = \varepsilon \frac{\hat{u_i}(t,\boldsymbol{\kappa})}{\sum_{||\boldsymbol{\kappa}||=\kappa_f} ||\hat{u_i}(t,\boldsymbol{\kappa})||^2} \delta(||\boldsymbol{\kappa}|| - \kappa_f), \tag{7}$$

where κ_f is the forced wavenumber has been used in (2). The injected energy per unit mass and time ε is equal to the mean energy dissipation rate when statistically steady conditions are achieved. A recently proposed numerical method [22, 23], which uses forward and inverse non-uniform fast Fourier transforms with a basis of fourth order B-splines, is implemented to interpolate fluid variables at particle positions and to compute the particle thermal feedback (6). An explicit exponential integrator of second order is used for the time integration of both the continuous phase, equations (1–3), and the discrete phase, equations (4). Please, refer to ref. [22, 23] for more details.

In this work, the only direct interaction between the particles occurs through elastic collisions. A binary collision takes place when the distance between the centres of a couple of particles matches their diameter. To incorporate collisions into the numerical simulation, we employ a first-order reconstruction of the particle trajectories, so that the p-th and q-th particles collide within a time step, $t \in [t_n, t_{n+1})$, if equation

$$||(1-\tilde{t})(\boldsymbol{x}_p(t_n) - (\boldsymbol{x}_q(t_n)) + \tilde{t}(\boldsymbol{x}_p(t_{n+1}) - (\boldsymbol{x}_q(t_{n+1}))|| = 2r_p, \tag{8}$$

where $\tilde{t} = (t-t_n)/\Delta t$, has a real solution $\tilde{t}$ in the interval $[0, 1)$. When this happens, particles continue their motion for the remaining part of the time-step with the velocity obtained after the collision, determined by momentum and energy conservation. It is supposed that particles do not exchange heat during the impact. Computationally, a direct detection of collisions can be highly expensive and impractical when the number of particles N_p is large, because the number of operations is of order $O({N_p}^2)$. Therefore, we use an alternative approach, which involves sorting particles into smaller boxes and searching for collisions within each box [24], a more practical and computationally feasible solution. Any potential missing arising from the box boundaries is avoided by repeating the algorithm after having shifted the boxes. Non binary collisions are not taken into consideration by this procedure.

3. Results and discussion

In this section, we compare the turbulent heat transport in the presence of colliding and non-colliding particles in the parameter range described in section 2.2 in the two-way coupling regime. A snapshot of a thin layer normal to the initial interface, showing particles coloured according to their temperature, is illustrated in figure 1. Particles move across the layer separating the two regions at different temperatures, advected by the flow and gaining and losing heat in the process. After about one timescale $\tau = \ell/u'$, this

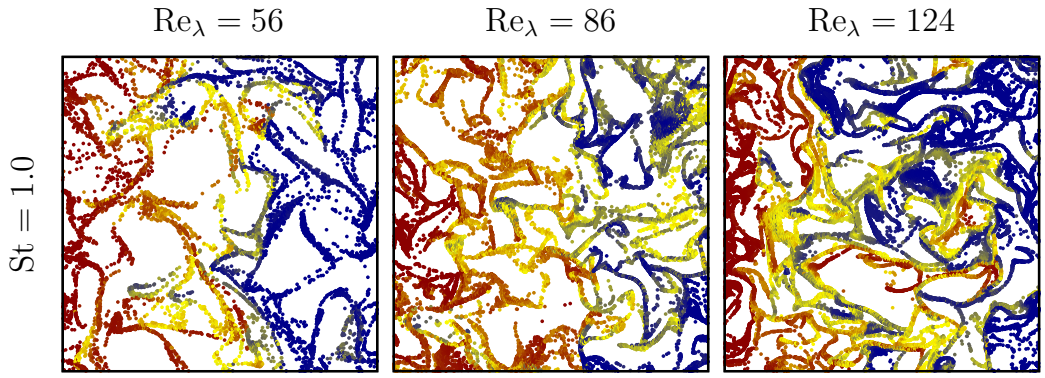

Figure 1. Visualization of particles in the collisional regime at $t/\tau = 3$, $\tau = \ell/u'$ in a small slab around a plane of (x_1, x_3). Particles are drawn not to scale and coloured in accordance with their temperature, from blue (lowest temperature) to red (maximum temperature).

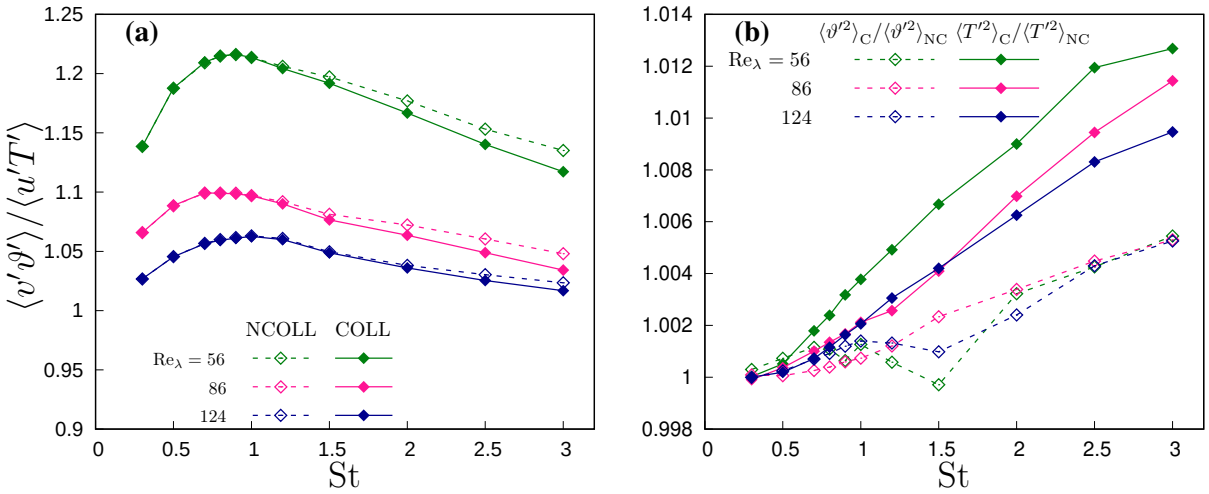

Figure 2. (a) Particle to fluid velocity-temperature correlation ratio as a function of St at different Re_λ (solid lines: collisional regime, dashed lines: collisionless). (b) Effect of collisions on fluid (continuous line) and particle (dashed lines) temperature variance as a function of St.

flow becomes self-similar: all the fluid and particle temperature statistics collapse, up to the numerical uncertainty, when they are rescaled with the thickness of mixing layer δ extracted from the mean temperature distribution, $\delta(t) = (T_1 - T_2)/\max\{|\partial T/\partial x_3|\}$, which shows an almost diffusive growth [18, 19]. The high fluid and particle temperature variance generated in the initial timescale decays as $1/\delta$ in this stage of evolution, while their ratio remains constant. Non-binary collisions are not taken into consideration.

Collisions produce a slightly reduction of the variance of particle temperature when compared to fluid temperature variance, in particular for particles with higher inertia [19]. The particle scattering induced by collisions changes the temperature variance. As illustrated in figure 2(b), in presence of collisions, the particle thermal feedback produces a more pronounced increase in fluid temperature variance compared to particle variance. This effect is particularly evident at large Stokes numbers. Although the difference is relatively small in present simulations, it becomes significant in terms of its implications at higher volume fractions, where collisions are more frequent and thermal feedback more intense. From equation

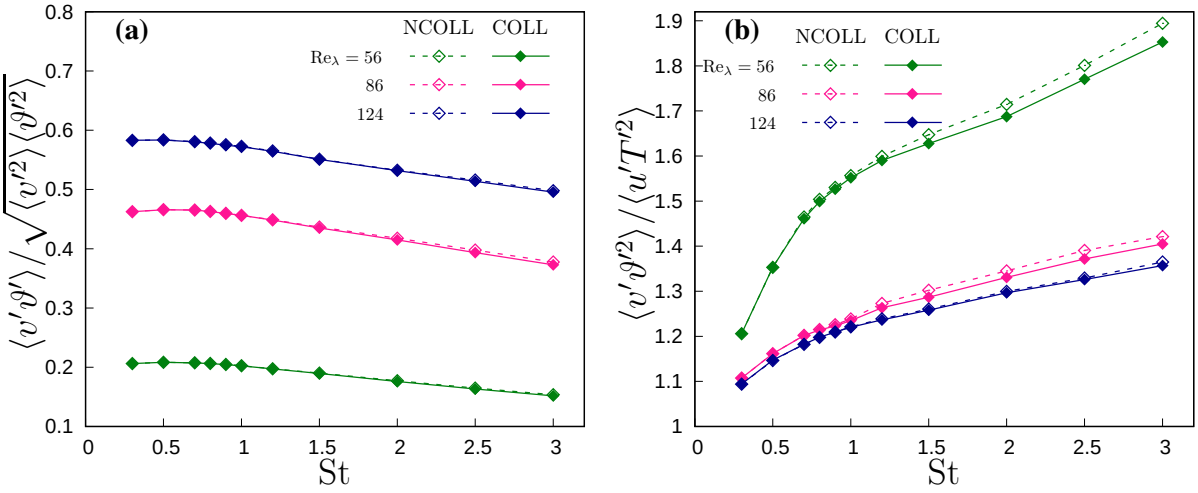

Figure 3. (a) Particle velocity-temperature correlation function as a function of the St. (b) Normalized particle temperature variance flow in the inhomogeneous direction x_3.

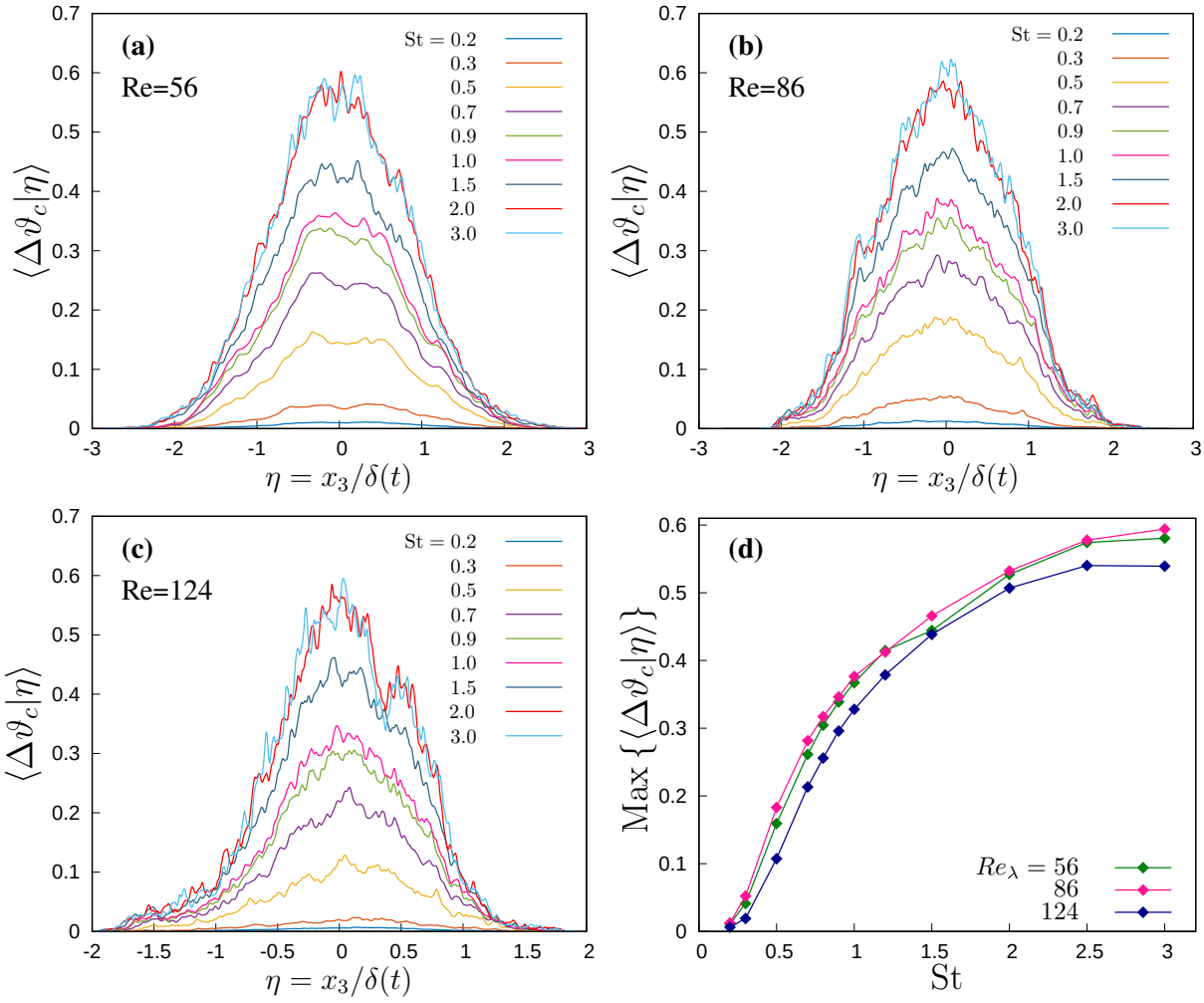

Figure 4. (a),(b),(c) average of $\Delta\vartheta_c = |\vartheta_a - \vartheta_b|$, where ϑ_a and ϑ_b denote the temperatures of the colliding particles, conditioned at the normalized position η of the collision, (d) maximum value of $\langle \Delta\vartheta_c|\eta\rangle$ as a function of St at different Re$_\lambda$.

(3), the overall mean heat flux in the inhomogeneous direction x_3 is

$$\dot{q} = -\lambda \frac{\partial \langle T \rangle}{\partial x_3} + \rho_0 c_{p0} \langle u_3' T' \rangle + \varphi \rho_p c_{pp} \langle v_3' \vartheta' \rangle \tag{9}$$

that is, the sum of the diffusive heat transfer, the fluid convective part, and the particle contribution [18]. The ratio between particle and fluid temperature-velocity correlation gives the particles relative contribution to the mean heat transfer. Figure 2(a) shows this ratio, computed in the centre of the mixing layer where these correlations have their maximum, as a function of St for three simulated Re_λ. The maximum occurs for a Stokes number around one at all Reynolds numbers both in collisional and collisionless regimes, in correspondence of the more intense clustering. Since the ratio between thermal and inertial relaxation times is fixed, in the tracer limit particles behave both dynamically and thermally as passive tracers and we have $\langle v_3' \vartheta' \rangle / \langle u_3' T' \rangle \to 1$ as $\mathrm{St} \to 0^+$. On the other side, in the infinite inertia limit, $\mathrm{St} \to \infty$, particles velocity and temperature tend to become independent of local flow structures, leading to a gradual reduction of $\langle v_3' \vartheta' \rangle / \langle u_3' T' \rangle$. Particle collisions have a negligible influence on fluid convective heat transfer. This implies that, within the examined volume fraction range, the collision-induced deviation from particles Lagrangian path has a mild effect on their average thermal feedback on the fluid. This is in agreement with Carbone et. al [6], who suggest two-way coupling and collision have a very weak effect on heat exchange between fluid and particle at high St. However, collisions do reduce the correlation between particle velocity and temperature, thereby limiting their capacity to transport heat over distances of the order of the mixing thickness. Given the increase in the collision frequency of larger particles which has been observed in [20], the impact on the turbulent heat flux in direction x_3 becomes more apparent as St increases [19, 20].

We can relate the observed attenuation of the correlation of particle temperature-velocity to the sling effect that produces interpenetration of particle trajectories from far zones in the inhomogeneous direction, therefore with very different temperatures, enhancing collisions which produces a scatter of the v_3 velocity component, thus reducing the $\langle v_3' \vartheta' \rangle$. Moreover, for large particles, this is associated, as explained by Carbone et. al [6], with the formation of thermal caustics, where particles with a very different temperature are gathered. Since we fixed the thermal Stokes to Stokes number ratio, these two simultaneous mechanisms act in the same way resulting in a dynamical and thermal decorrelation from local flow. Consequently, even if the ability of particles heat exchange with each other increases due to the sling effect and thermal caustic, but their ability to transfer heat with fluid decreases and we can see the reduction in overall heat transfer in direction x_3 in collisional regime at large St. On one hand, due to high thermal inertia, particles avoid transferring heat with surrounding fluid, collision is also boosting this manner, on the other hand, particle momentum exchange with other particles reduces their ability to carry heat to the other distant regions, then causing a heat flux attenuation in thermal mixing layer. Information about the particle ability to transport heat can also be inferred from the velocity-temperature correlation function $\langle v_3' \vartheta' \rangle / \sqrt{\langle v_3'^2 \rangle \langle \vartheta'^2 \rangle}$, which reduces with St, as shown in figure 3(a). The reason is that larger particles with higher inertia tend not to be correlated with local fluid velocity field and resulting in lower correlation function. Conversely, the correlation function has the highest value for lowest Stokes number implying that particles at this Stokes number are highly correlated with fluid field. Particle temperature variance flux becomes much larger than fluid temperature variance, figure 3(b) as the Stokes number increase, as particles can move over longer distance keeping their temperature. Even in this case, the collisional scattering reduces this flux. Indeed, an increase of the colliding particles temperature difference with the St can be observed, see figures 4(a),(b),(c) an indication that a higher particle inertia makes possible collisions between particles coming from very far zones, letting them pass through the fluid temperature fronts [6], while they can keep their temperature due to their thermal inertia. The temperature difference at collision has a minor dependence on the Reynolds number, but increases with the Stokes number, approaching a constant value for St larger than 2 (figure 4(d)). As observed in [6], inertial particles relative temperature difference depends non locally on the fluid small-scale temperature structure function experienced along their respective trajectories so that even at small scale separation

their temperature difference can significantly exceed the small-scale local fluid temperature difference. Since it has been found that collisions event between particles with larger inertia are, as expected, more likely, the impact on the temperature-velocity correlation increases as St increases [20].

4. Conclusion

This study delves into some aspects of the modification of turbulent heat transport induced by particle collisions. Collision-induced scattering significantly amplifies fluid temperature variance compared to particle variance, notably at larger Stokes numbers, through particle feedback, and decrease the correlation between particle velocity and temperature, limiting their long-distance heat transport efficiency, but the effect is globally a minor one. With increasing Stokes numbers, collision frequency rises, influencing turbulent heat flux. This decline in particle temperature-velocity correlation is linked to the sling effect, boosting collisions and diminishing heat transfer capacity. Overall, our findings highlight the intricate interplay of particle collisions, inertia, and their interaction with fluid, revealing nuances in heat transport mechanisms. They underscore the role of collision dynamics and particle characteristics in shaping turbulent heat flux within particle-laden flows.

5. References

[1] Pumir A and Wilkinson M 2016 *Annu. Rev. Condens. Matter Phys.* **7** 141–170
[2] Zonta F, Marchioli C and Soldati A 2008 *Acta Mech.* **195** 305–326
[3] Kuerten J G M, van der Geld C W M and Geurts B J 2011 *Phys. Fluids* **23** 123301
[4] Rousta F and Lessani B 2020 *Int. Commun. Heat Mass Transf.* **112** 104475
[5] Béc J, Homann H and Krstulovic G 2014 *Phys. Rev. Lett.* **112**(23) 234503
[6] Carbone M, Bragg A D and Iovieno M 2019 *J. Fluid Mech.* **881** 679–721
[7] Saito I, Watanabe T and Gotoh T 2022 *J. Fluid Mech.* **931** A6
[8] Saffman P G and Turner J S 1956 *J. Fluid Mech.* **1** 16–30
[9] Sundaram S and Collins L r 1997 *J. Fluid Mech.* **335** 75–109
[10] Abrahamson J 1975 *Chem. Eng. Sci.* **30** 1371–1379
[11] Zaichik I I and Pershukov V A 1995 *Fluid Dyn.* **30** 49–63
[12] Wang L P, Wexler A and Zhou Y 2000 *J. Fluid Mech.* **415** 117 – 153
[13] Sommerfeld M 2001 *Int. J. Multiph. Flow* **27** 1829–1858
[14] Johnson P 2019 *Int. J. Multiph. Flow* **124** 103182
[15] Kuerten J and Vreman A 2016 *Int. J. Multiphase Flow* **87** 66–79
[16] Jiang F, Wang H, Liu Y, Qi G, Al-Rawni A E, Nkomazana P and Li X 2021 *Powder Technol.* **381** 55–67
[17] Sun J and Chen M M 1988 *Int. J. Heat Mass Transfer* **31** 969–975
[18] Zandi Pour H R and Iovieno M 2022 *Fluids* **7** 345
[19] Zandi Pour H R and Iovieno M 2023 *8th World Congress on Momentum, Heat and Mass Transfer*
[20] Zandi Pour H R and Iovieno M 2023 *J. Fluid Flow Heat Mass Transf.* **10** 140–149
[21] Maxey M R and Riley J J 1983 *Phys. Fluids* **26** 883–889
[22] Carbone M and Iovieno M 2018 *WIT Trans. Eng. Sci.* **120** 237–248
[23] Carbone M and Iovieno M 2020 *Int. J. Saf. Sec. Eng.* **10** 191–200
[24] Onishi R, Takahashi K and Vassilicos J C 2013 *J. Comput Phys.* **242** 809–827

Acknowledgements

The authors would like to gratefully acknowledge PRACE for having awarded them access to high performance computing and special storage resources at HPC Vega-IZUM, Maribor, Slovenia under the PRACE EuroHPC Development Access project 2023D02-007.